Photoluminescence Quantum Yield of Single-Wall Carbon Nanotubes Corrected for the Photon Reabsorption Effect

Xiaojun Wei,[†] Takeshi Tanaka,[‡] Shilong Li,[†,§] Mayumi Tsuzuki,[‡] Guowei Wang,[‡] Zhihui Yao,[†] Linhai Li,[†,§] Yohei Yomogida,[∥] Atsushi Hirano,[‡] Huaping Liu,[†,§] and Hiromichi Kataura*,[‡]

[†]Beijing National Laboratory for Condensed Matter Physics, Institute of Physics, Chinese Academy of Sciences, Beijing 100190, China

[‡]Nanomaterials Research Institute, National Institute of Advanced Industrial Science and Technology (AIST), Tsukuba, Ibaraki 305-8565, Japan

[§]Department of Physical Science, University of Chinese Academy of Sciences, Beijing 100049, China

[∥]Department of Physics, Faculty of Science, Tokyo Metropolitan University, Hachioji, Tokyo 192-0397, Japan

S *Supporting Information*

ABSTRACT: Photoluminescence (PL) from single-wall carbon nanotubes (SWCNTs) enables structural identification, but to derive the content rate of the specific chirality species it is necessary to know the quantum yield of each chirality. However, in the PL of SWCNTs, because the Stokes shift is small, the photon reabsorption effect is dominant and the apparent PL spectral shape and emission intensity are greatly modified depending on the concentration. This problem makes quantitative identification of SWCNTs by PL difficult. In this study, the concentration dependence of the PL of SWCNTs separated into a few chiralities was analyzed in detail, including the effect of reabsorption. It is clear that all changes in the PL spectrum occurring in the high concentration range can be explained simply by the reabsorption effect, and additional effects such as Coulomb interactions between SWCNTs can be negligible. Furthermore, a reliable quantum yield was derived from the emission intensity corrected for the reabsorption effect. The PL quantum yield varied with SWCNT chirality and exhibited a clear "family pattern". This is consistent with the theoretical report showing that the chirality-dependent PL quantum yield is dominated mainly by relaxation by optical phonons from E_{22} to E_{11}.

KEYWORDS: Carbon nanotube, photoluminescence, quantum yield, photon reabsorption, chirality dependence
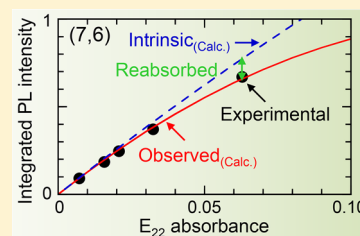
Single-wall carbon nanotubes (SWCNTs) have a tubular graphene structure and change their one-dimensional (1D) electronic properties depending on the atomic arrangement defined by a pair of chiral indices (n,m).[1] As a typical example of 1D confinement effects, semiconducting SWCNTs exhibit (n,m)-specific near-infrared E_{11} 1D-exciton photoluminescence (PL) for E_{22} excitation.[2] Using a pair of E_{11} PL emission and E_{22} excitation wavelengths, we can identify (n,m) species of the SWCNTs contained in a sample using the "family pattern" of SWCNTs. The PL intensity is also often used to deduce the abundance of specific (n,m) species in an as-grown or (n,m)-sorted sample.[3−10] In the case of the quantitative evaluation of (n,m) abundance, however, the PL quantum yield of each (n,m) species is necessary to derive the relative abundance of (n,m) species from the PL intensity. Previously, a theoretical study demonstrated that the PL quantum yield is strongly dependent on the structural factors of SWCNTs, such as diameter, chiral angle, family number ($2n + m$), and mod($2n + m$, 3), where SWCNTs with mod($2n + m$, 3) = 1 and 2 are called Type I and Type II, respectively.[11] In contrast, Tsyboulski et al. measured the PL cross section per carbon atom for a few (n,m) species using single-SWCNT microphotometry and revealed that the PL quantum yield generally increases with decreasing SWCNT diameter.[12] In

addition, Mouri et al. also observed diameter-dependent PL quantum yields using several SWCNT sources, such as HiPco and CoMoCAT.[13] However, in the above experiments, the photon reabsorption effect[14−16] was not considered for the estimation of PL intensities and further quantum yields. Because the Stokes shift is very small in this system, the photon reabsorption effect could be a serious problem. In fact, the reported experimental results[12,13] did not reproduce the "family pattern" of the quantum yields predicted by theoretical calculations.[11] In this study, we investigated the effect of photon reabsorption on PL characteristics for (n,m)-sorted semiconducting SWCNTs. We have revealed that the apparent PL spectral change at high SWCNT concentrations is purely caused by a simple photon reabsorption effect, and additional effects such as Coulomb interactions between SWCNTs can be negligible. This simple situation enabled us to analyze intrinsic PL intensities. We obtained the PL quantum yields corrected for the photon reabsorption effect and then found a clear family pattern for the first time, which agrees well with the theoretical prediction.
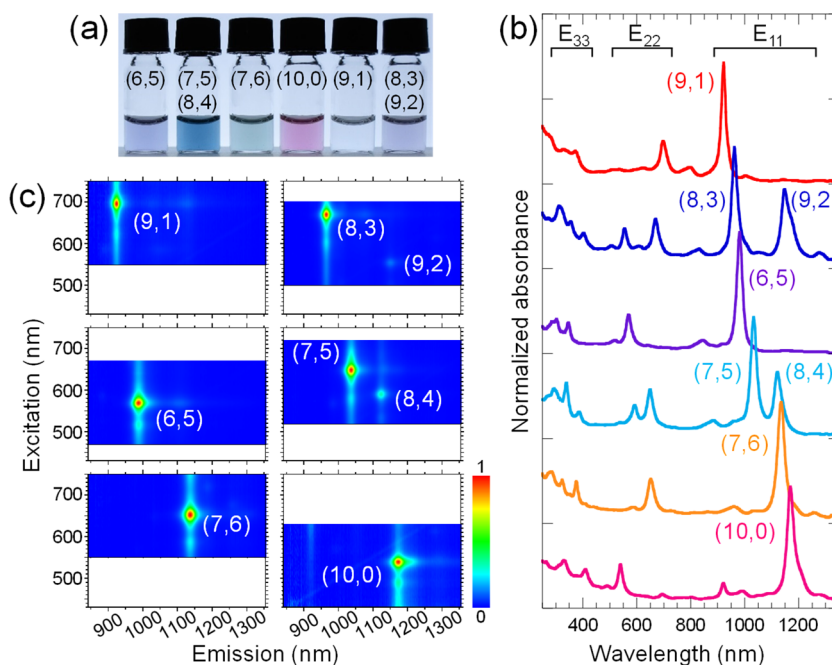
Figure 1. (a) Photograph of six concentrated SWCNT solutions. (b) Optical absorption spectra of six diluted SWCNT solutions. Each spectrum is normalized by the maximum absorbance at E_{11}, and the spectra are offset vertically for comparison. (c) Typical PL excitation−emission spectral maps of six diluted SWCNT solutions. Intensities are normalized at each maximum.
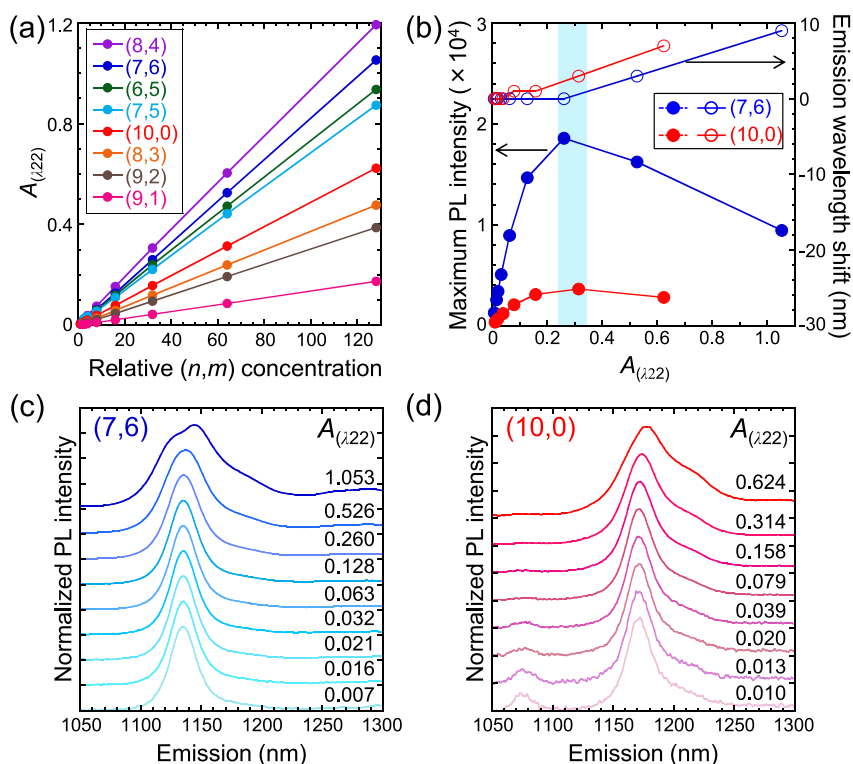

Figure 2. (a) Plots of maximum E_{22} absorbance ($A_{(\lambda 22)}$) of each (n,m) SWCNT as a function of the relative (n,m) concentration for the most dilute sample. (b) Plots of the observed maximum PL intensities (left axis) and PL peak shifts (right axis) for (7,6) and (10,0) SWCNTs as a function of $A_{(\lambda 22)}$. (c,d) PL spectra of the SWCNT solutions with an excitation wavelength of 652 nm for (7,6) SWCNT and 540 nm for (10,0) SWCNT at different $A_{(\lambda 22)}$ values, where the PL intensities are normalized by each maximum value and the spectra are offset for comparison. Each emission spectrum was measured 5 times, and the averaged spectrum was adopted in this work. The weak peaks observed at 1080 nm in the PL spectra of the dilute (10,0) samples are attributed to second-order Rayleigh scattering.

Because PL analysis for a mixed chirality sample is very difficult, we prepared Type I ($2n + m = 19$) species (i.e., (7,5), (8,3), and (9,1)), Type II ($2n + m = 20$) species (i.e., (7,6),

(8,4), (9,2), and (10,0)), and the most often examined (6,5) species, which were sorted using gel column chromatography with multiple surfactants.[17−20] Different from previous gel

column chromatography with a single surfactant,[21−24] in the current sorting procedure, each (n,m) SWCNT was dispersed in different surfactant mixtures. To exclude the influence of the surfactant on the PL intensity, the surfactants of all the SWCNT solutions were replaced with the identical surfactant in 0.5 wt % sodium cholate (SC) using a cross-flow filtration system (AKTA flux s, GE Healthcare) equipped with a hollow fiber cartridge (surface area 26 cm², Type 500 K, GE Healthcare). After replacement of the surfactant, the SWCNTs in each solution were concentrated using a centrifugal filter unit (Amicon Ultra-15 with Ultracel-100 K membrane, Merck Millipore) at 3000*g*. To prepare the SWCNT solutions with different concentrations, the concentrated SWCNT solution was diluted 2, 4, 8, 16, 32, 48, 64, and 128 times using a 0.5 wt % SC solution.

Figure 1a shows a photograph of six concentrated SWCNT solutions. The different colors of the solutions indicate different (n,m) components. The samples have light colors, but the concentrations are high enough to show the typical photon reabsorption effect. Figure 1b shows the optical absorption spectra of diluted SWCNT solutions measured by an ultraviolet−visible-infrared spectrophotometer (UV-3600, Shimadzu) using a quartz cuvette with a path length of 10 mm. Each spectrum exhibits a series of sharp absorption peaks, corresponding to E_{11}, E_{22}, and E_{33} transitions, with significantly low background absorption, which strongly suggests high-level removal of metallic SWCNTs and amorphous carbon. The SWCNTs contained in the samples were identified as (9,1), (8,3), (9,2), (6,5), (7,5), (8,4), (7,6), and (10,0) based on their E_{11} and E_{22} absorption peak wavelengths.[2,17,25,26] Figure 1c shows PL excitation−emission spectral maps of the diluted samples measured by a spectrophotometer (Nanolog, HORIBA) equipped with a liquid nitrogen-cooled InGaAs near-infrared array detector. The peak positions were consistent with the absorption spectra. As described later, these optical absorption spectra and PL spectral maps were used to derive the PL quantum yields. Importantly, two samples (the second and fourth samples from the top in Figure 1b) were not composed of single-(n,m) SWCNTs; nevertheless, these SWCNTs, i.e., a mixture of (8,3) and (9,2) and mixture of (7,5) and (8,4) could be subjected to analyses of their quantum yields because the E_{11} and E_{22} peaks of (8,3) and (7,5) do not overlap with those of the (9,2) and (8,4) SWCNTs, respectively. This assertion is confirmed by the PL spectral maps shown in Figure 1c, where the bright E_{11} peaks of (8,3) and (7,5) do not overlap with those of (9,2) and (8,4), respectively. It should be noted that the E_{11} absorption peak of (9,2) SWCNTs is unusually broad, which is partly induced by the wavelength shift (∼6 nm) of two enantiomers of (9,2) SWCNTs (Supporting Information, Figure S1). Although the wavelength shift should also appear in the E_{11} emission peak, this shift will not affect the analysis of PL quantum yield because we count the integrated PL intensity covering the entire E_{11} emission peak. Another possible reason is the contamination of tiny amount of (12,1) SWCNTs. Since the E_{22} excitation wavelength of (9,2) is different from that of (12,1), analysis of PL quantum yield of (9,2) SWCNTs is not affected by the contamination.

Figure 2a shows the absorbance at the E_{22} transition $(A_{(\lambda 22)})$ of each (n,m) SWCNT as a function of the relative (n,m) SWCNT concentration obtained from a dilution ratio from the starting solutions. Clearly, $A_{(\lambda 22)}$ increases proportionally to the relative SWCNT concentration, while the full width at half-

maximum of the E_{22} absorption peaks was independent of the SWCNT concentration (not shown). These results indicate that the optical absorbance at the E_{22} transition $A_{(\lambda 22)}$ is a good scale of the SWCNT concentration. In contrast, the PL results exhibited different characteristics. Figure 2b shows the maximum PL intensities and peak shifts for near-armchair (7,6) and zigzag (10,0) SWCNTs as a function of $A_{(\lambda 22)}$, which is proportional to the SWCNT concentration (Figure 2a). In the low absorbance region (<0.3), i.e., in the low SWCNT concentration region, the PL intensity increased with increasing $A_{(\lambda 22)}$, and the peak wavelength did not show a large change. In the high absorbance region (>0.3), however, the PL intensity decreased with increasing $A_{(\lambda 22)}$, and the peak wavelength shifted to a longer wavelength. Figure 2c and d shows the PL spectra of the (7,6) and (10,0) SWCNT solutions at each $A_{(\lambda 22)}$ corresponding to the plots in Figure 2b. Here, to observe the spectral shape change, the PL spectra were normalized by each maximum intensity. With increasing $A_{(\lambda 22)}$, the apparent E_{11} PL peaks became broader, and the shoulders at 1190 nm for (7,6) and at 1220 nm for (10,0) SWCNTs became more obvious. In addition, E_{11} PL peak splitting was observed for the (7,6) SWCNT at a relatively high $A_{(\lambda 22)}$ value of 1.053. Similar spectral changes were also observed for the other (n,m) species at high $A_{(\lambda 22)}$ (Supporting Information, Figure S2). This result demonstrates that the optical absorbance is an important factor in the PL characteristic of SWCNTs. Before performing a detailed analysis, we note that all SWCNT samples showed unusual maximal PL intensities at almost the same $A_{(\lambda 22)}$ value (0.25−0.35) (Supporting Information, Figure S3). This unusual phenomenon was caused by the optical path design of our PL measuring system. Since our system is designed for a low absorbance solution, the focal point of the PL collector lens is at the center of the optical cell, which means that the detector does not uniformly collect the PL signal from the full optical cell but rather dominantly collects the signal from the center of the optical cell.[27] This difference is the reason why the PL intensity decreased after reaching the maximum. More details will be described below. In addition, the attenuation of the PL intensity induced by photon reabsorption on the oxide-induced E^*_{11} state[28−32] is thought to be very weak, which is consistent with the low optical absorbance at the wavelengths of E^*_{11} (Supporting Information, Figure S4).

For the analysis of the PL intensities, we must consider photon reabsorption[14−16] because the E_{11} optical absorbance is significantly large and the Stokes shift is very small. As the first step, the reabsorbed optical spectrum $(I_{reabs}(\lambda))$ was obtained by simply subtracting the experimentally observed PL spectrum $(I_{obs}(\lambda))$ from the intrinsic spectrum $(I_{int}(\lambda))$, $(I_{reabs}(\lambda) = I_{int}(\lambda) - I_{obs}(\lambda))$. For this analysis, we need the intrinsic spectrum $(I_{int}(\lambda))$. In this work, we assumed that reabsorption is negligible for the most dilute solutions that correspond to $A_{(\lambda 22)}$ of 0.007 for (7,6) and 0.010 for (10,0) in Figure 2c and d. We used the observed PL spectrum $(I_{obs}(\lambda))$ for the most dilute solutions as the intrinsic PL spectrum $(I_{int}(\lambda))$. We defined the normalized intrinsic spectrum $(I_{int}^{normal}(\lambda))$, the normalized observed spectrum $(I_{obs}^{normal}(\lambda))$, and the normalized reabsorption spectrum $(I_{reabs}^{normal}(\lambda))$ as follows:

$$I_{int}^{normal}(\lambda) = I_{obs}^{dilute}(\lambda)/A_{(\lambda 22)}^{dilute} \tag{1}$$

$$I_{obs}^{normal}(\lambda) = I_{obs}(\lambda)/A_{(\lambda 22)} \tag{2}$$

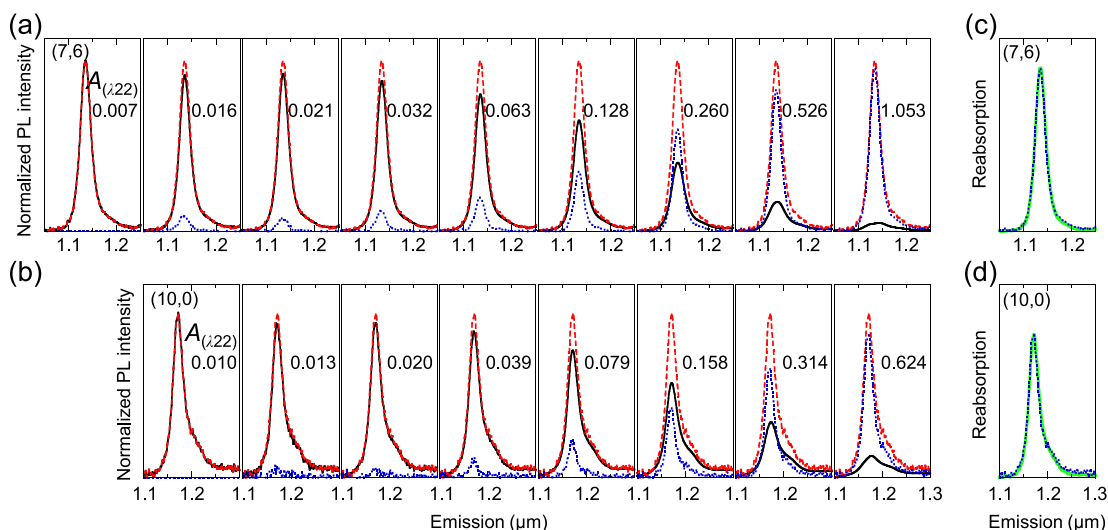**Figure 3.** (a,b) Intrinsic spectra ($I_{int}^{normal}(\lambda)$, red dashed curves), observed spectra ($I_{obs}^{normal}(\lambda)$, black solid curves), and reabsorption spectra ($I_{reabs}^{normal}(\lambda)$, blue dotted curves) with different concentrations ($A_{(\lambda22)}$ values) of (7,6) (a) and (10,0) (b) solutions. (c,d) Reabsorption spectra calculated from the measured optical absorption spectrum for the light source of the intrinsic PL emission spectrum (green solid curves), accompanied by the reabsorption spectra $I_{reabs}^{normal}(\lambda)$ (blue dotted curves), refer to the rightmost spectrum in Figure 3a and b for comparison.

$$I_{reabs}^{normal}(\lambda) = I_{int}^{normal}(\lambda) - I_{obs}^{normal}(\lambda) \qquad (3)$$

where $I_{obs}^{dilute}(\lambda)$ and $A_{(\lambda22)}^{dilute}$ are the observed spectrum and optical absorbance at E$_{22}$ for the most dilute SWCNT solutions, respectively.

Figure 3a and b shows the normalized intrinsic PL spectra ($I_{int}^{normal}(\lambda)$, red dashed curves) as well as the normalized observed spectra ($I_{obs}^{normal}(\lambda)$, black curves, refer to Figure 2c and 2d) for different concentrations of (7,6) and (10,0) solutions. The normalized reabsorption spectra ($I_{reabs}^{normal}(\lambda)$) were obtained from them using eq 3 and are indicated in Figure 3 (blue dotted curves). The normalized reabsorption intensity increased with increasing SWCNT concentration. This increase is natural because reabsorption should be proportional to the SWCNT concentration. It is important to note that the spectral shapes of the intrinsic and the reabsorbed PL did not change for all measured concentrations (Supporting Information, Figure S5). Because the light source in the reabsorption process is the PL emission, the reabsorption spectrum is modified from the optical absorption spectrum by the light source spectrum. To compare the reabsorption spectrum with the optical absorption spectrum, we calculated the reabsorption spectrum from the measured optical absorption spectrum for the intrinsic PL emission spectrum. Figure 3c and d shows the reabsorption spectra calculated from the measured optical absorption spectra and intrinsic PL spectra, which perfectly agree with the reabsorption spectra obtained from the PL measurements. This result means that the changes in the observed PL spectra are ascribed to the pure reabsorption process. The broadening and splitting of the PL spectra observed for high concentrations, as shown in Figure 2c and 2d, are well reproduced by a simple reabsorption effect. For the other (n,m) species, we obtained similar results with (7,6) and (10,0) species (Supporting Information, Figures S6−S11), where all PL spectral changes could be explained by the reabsorption effect. In previous studies, the PL spectral change at high SWCNT concentrations was explained by the local environmental change around the SWCNTs, including the dielectric constant, exciton energy transfer, and exciton−phonon interaction.[33−35]

At least within the SWCNT concentrations examined in this work, however, the reabsorption effect enables us to fully interpret the $A_{(\lambda22)}$-dependent PL spectral changes, indicating that the other factors caused by interactions between SWCNTS as described above are negligible.

We identified the quantum yield of each (n,m) SWCNT by analyzing the $A_{(\lambda22)}$-dependent PL spectral changes as described below. We considered the process of photon propagation into a uniform SWCNT solution in the PL measurement system: first, the excitation light is incident into the SWCNT solution; second, the generated emission light passes through the SWCNT solution; finally, the emission light is collected by a detector fixed at a constant angle against the excitation light direction. When the excitation condition is fixed, the integrals of $I_{int}(\lambda)$, i.e., the intrinsic PL peak areas, without reabsorption, should depend on $A_{(\lambda22)}$ as follows:

$$\int I_{int}(\lambda)\, d\lambda = \frac{\Omega}{4\pi} I_0 \phi (1 - \exp(-A_{(\lambda22)})) \qquad (4)$$

where $\Omega/4\pi$ indicates the collection solid angle of the detector, I_0 indicates the excitation light intensity, and ϕ indicates the PL quantum yield of a specific (n,m) SWCNT (see details in the Supporting Information). The integrals of $I_{obs}(\lambda)$ at low values of $A_{(\lambda22)}$, typically less than 0.1, can be approximated by the following equation (see details in the Supporting Information):

$$\int I_{obs}(\lambda)\, d\lambda = \frac{\Omega}{4\pi} I_0 \phi A_{(\lambda22)}$$
$$- \frac{\Omega}{8\pi} I_0 \phi \left(\int \left(1 + \frac{A_{(\lambda)}}{A_{(\lambda22)}} \right) f(\lambda)\, d\lambda \right) A_{(\lambda22)}^2 \qquad (5)$$

where $A_{(\lambda)}$ and $f(\lambda)$ indicate the absorption spectrum and the normalized intrinsic PL spectrum (whose areas are normalized to unity, $\int_{\lambda11} f(\lambda) = 1$), respectively. Importantly, because all raw intensity data have been corrected on the basis of the spectrum of the lamp and the collection solid angle was fixed,
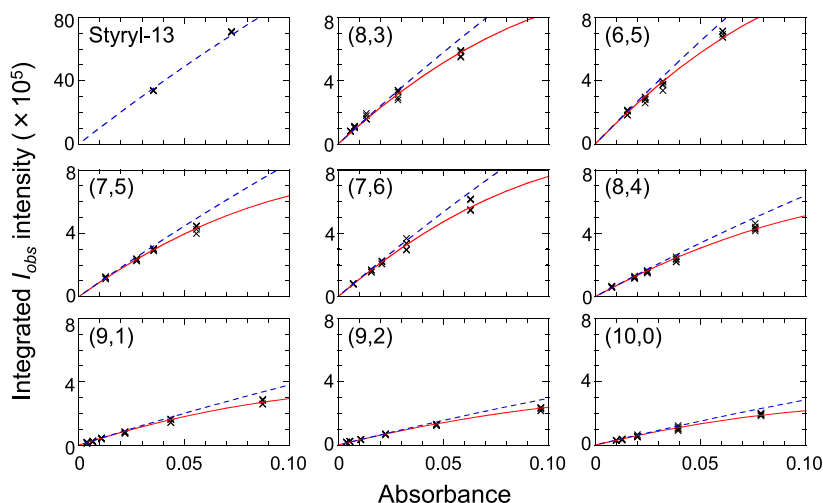
Figure 4. Plots of the integrated I_{obs} intensity (cross symbols) for Styryl-13 and eight (n,m) samples as a function of optical absorbance ($A_{(\lambda 22)}$ for SWCNTs), in which the values for SWCNTs have been corrected with the absorption of the solvent using the rate of decrease in the emission intensity presented in Figure S13. Blue dashed and red solid curves indicate the fitting results based on eqs 4 and 5, respectively.

the values of I_0 and $\Omega/4\pi$ were treated as constant in these calculations.

Equation 5 incorporates the reabsorption effects by SWCNTs, but we need to incorporate the absorption of solvent, H_2O in near-infrared region. To clarify the influence of the solvent on the emission intensity, the original SC/H_2O solvent was replaced with SC/D_2O solvent. The concentrations of SWCNTs dispersed in SC/H_2O and SC/D_2O solvents were adjusted to be consistent by assuming that the absorption cross section of the specific (n,m) species is identical for SC/H_2O and SC/D_2O solvents (Supporting Information, Figure S12a). As a result, a significant decrease in the integrated PL intensity was observed for the SC/H_2O (denoted as I_{H2O}) compared with SC/D_2O (denoted as I_{D2O}) solvent (Supporting Information, Figure S12b). The rate of decrease (defined as $\eta = (I_{D2O} - I_{H2O})/I_{D2O}$) is obviously dependent on the emission wavelength within a range from 8.4 to 49.8%, which agrees with the absorption of H_2O (Supporting Information, Figure S13). By assuming that the absorption of D_2O is negligible, the corrected PL intensity can be estimated by incorporating the absorption of H_2O.

To correctly evaluate PL quantum yield, the excitation and emission wavelengths of reference dye are very important to compensate the spectroscopic instrument functions. Indeed, Crochet et al. used Styryl-13 as the reference dye to obtain PL quantum yield of (6,5) SWCNTs, because both excitation and emission wavelengths of Styryl-13 match with that of (6,5).[34] For the other (n,m) species, therefore, appropriate reference dyes that match with their excitation and emission wavelengths should be prepared. In the present work, however, we used Styryl-13 as reference dye for all chiralities. Because the sensitivity of the InGaAs detector, transmittance of the monochromator, and efficiency of the other optical components in our PL measurement equipment were totally corrected by calibration function obtained by using a standard lamp, we can compare PL intensity of each species without farther corrections. Also, intensity of incident light was recorded by sensitivity-calibrated Si detector and PL intensity was normalized by the incident light intensity. (details are described in the optical measurements in the Supporting Information). In this condition, all emission intensities excited

by any wavelength are comparable. Therefore, the Styryl-13 is considered to be suitable for evaluating the PL quantum yield of distinct (n,m) SWCNTs in our case. As shown in Figure S14, Styryl-13 (Radiant Dyes Laser & Accessories GmbH, laser dye LDS 925) dissolved in methanol has a large Stokes shift (ca. 341 nm); therefore, we assumed that there is no reabsorption in a solution of Styryl-13. In other words, the integrated I_{obs} is identical to the integrated I_{int} for Styryl-13. Figure 4 shows plots of the integrated I_{obs} intensity, i.e., PL peak area, for Styryl-13 as a function of the values of the absorbance peaks and plots for the eight (n,m) species examined as a function of each $A_{(\lambda 22)}$, where the values for SWCNTs have been corrected with the absorption of the solvent using the decrease ratio in the emission intensity presented in Figure S13. As expected from eq 4, the integrated I_{obs} intensities of Styryl-13 increased nonlinearly with increasing values of the absorbance peaks. We fit eq 4 to the integrated I_{obs} intensities of Styryl-13 (blue dashed curve) and then determined the value of $\Omega I_0 \phi/4\pi$; we estimated the value of $\Omega I_0/4\pi$ (4.1×10^8) by adopting a quantum yield of 11% for Styryl-13, which was reported previously.[29,34] For the SWCNTs, we fit eq 5 to the integrated I_{obs} intensities (red solid curves) and then determined the values of $\Omega I_0 \phi/4\pi$. We estimated the quantum yields per unit of absorbed photons of the SWCNTs using the value of $\Omega I_0/4\pi$ determined above (Table S1). In addition, we derived the integrated I_{int} intensities of the SWCNTs using the obtained parameters and eq 4 (blue dashed curves) because they could not have been measured experimentally. In addition, we calculated the curve of the observed PL intensity for the local volume at the center of the optical cell as a function of SWCNT concentration (Supporting Information, Figure S15a). As a result, the calculated curve reproduces our experimental observation that the PL intensity decreased after reaching the maximum, verifying our explanation. In addition, we found that the issue of focal collection does not affect the PL intensity for low SWCNT concentrations (Supporting Information, Figure S15b).

Since absorption cross section of each (n,m) species is different,[36,37] we have converted the PL quantum yields per unit of absorbed photons into that per carbon atom using a

theoretical formula of (n,m)-dependent optical oscillator strengths.[38] Table 1 summarizes the structural parameters

Table 1. Structural Parameters and Estimated PL Quantum Yields for Eight (n,m) Species[a]

(n,m)	family $(2n + m)$	diameter (nm)	chiral angle (degree)	λ_{11} (nm)[b]	λ_{22} (nm)[b]	ϕ (%) per carbon atom @ λ_{22} excitation[c]
(9,1)	19	0.747	5.21	922	698	0.36 ± 0.04
(8,3)	19	0.771	15.30	962	670	1.20 ± 0.08
(6,5)	17	0.747	27.00	982	570	1.40 ± 0.13
(7,5)	19	0.817	24.50	1034	650	1.04 ± 0.10
(8,4)	20	0.829	19.11	1122	592	0.86 ± 0.05
(7,6)	20	0.882	27.46	1136	652	1.40 ± 0.09
(9,2)	20	0.795	9.83	1148	556	0.37 ± 0.03
(10,0)	20	0.783	0.00	1170	540	0.35 ± 0.01

[a]λ_{11} and λ_{22} indicate the center wavelengths of the E_{11} and E_{22} transitions, respectively. [b]These values were estimated from optical absorption spectra, which contain ±2 nm error due to the wavelength accuracy of the spectrometer. [c]The uncertainties of these values were estimated by the fitting error (shown in Figure 4), the absorption of the solvent (shown in Figure S13), and the difference in PL quantum yield between two enantiomers (shown in Figure S16).

along with the estimated PL quantum yields per carbon atom (ϕ) for the examined eight (n,m) species. The PL quantum yields of the near-armchair species are similar to those reported in previous studies, although the quantum yields of near-zigzag and zigzag species have not been reported previously.[13,39−41] Since each (n,m) species of the SWCNTs used in this work was isolated from the same SWCNT dispersion prepared by the same processes, it is valid to compare their PL quantum yields. The maximum value of 1.40% for the (6,5) SWCNTs was as much as 3.9 times higher than the value of 0.36% for the (9,1) SWCNTs, even though these two species have the same diameter. In addition, although (7,6) SWCNTs and (10,0) SWCNTs belong to the same family 20, the yield of the near-armchair (7,6) SWCNTs is 4 times higher than that of the zigzag (10,0) SWCNTs. A large difference in the PL quantum yield between (8,3) and (9,2) SWCNTs was consistent with the fact that the observed PL intensity of the (8,3) SWCNTs is much stronger than that of (9,2) (Figure 1c), although their

$A_{(\lambda 22)}$ values are not significantly different from each other (Figure 1b). Generally, the PL intensities of zigzag species in the as-grown SWCNTs were significantly low compared to those of the other species,[2] which may be explained not only by the small abundance but also by the low quantum yield.

To examine the dependence of the PL quantum yields on SWCNT structures, the quantum yields listed in Table 1 were plotted as a function of the SWCNT diameter (Figure 5a). The PL quantum yield strongly changes depending on the (n,m) indices for both Type I and Type II species. For Type I ($2n + m = 19$) species, i.e., (7,5), (8,3), and (9,1) species, no monotonous chiral angle dependence was observed. For Type II ($2n + m = 20$) species, i.e., (7,6), (8,4), (9,2), and (10,0) species, the PL quantum yields decreased with decreasing chiral angle. Importantly, the PL quantum yields corrected on the basis of photon reabsorption exhibit an obvious family pattern, which is similar to that of the PL intensities predicted by the previous theoretical calculation (Figure 5c[11]), especially for chiral angle dependence in small diameter range. Although the theoretical calculation shows smaller PL intensity for Type II species than for Type I mainly due to smaller induced optical absorption in Type II SWCNTs,[11] our results show the PL quantum yield for Type I and Type II are comparable at small diameter range. Family pattern of PL intensity was also reported by Tsyboulski et al. using microscopic PL measurements on individual SWCNTs as shown in Figure 5b.[12] Their results also well reproduce theoretically predicted family behavior at slightly larger diameter range than our results. Interestingly, the family patterns in our present result (Figure 5a) and in the PL action cross sections (Figure 5b) complementarily reproduce theoretical results shown in Figure 5c. Theoretical calculation further showed that the PL intensity of semiconducting SWCNTs is mainly dominated by the relaxation process due to the longitudinal optical (LO) phonons from E_{22} to E_{11}.[11] The significantly low PL intensities of (9,1) and (11,0) species are originated from their low relaxation rates due to smaller energy separation between E_{22} and E_{11} than the LO phonon energy.[11] Although the experimentally obtained PL quantum yield of (9,1) species is also very low, it is still comparable to that of (8,3) species, which is different from their PL intensities in theoretical calculations. This difference can be explained by the difference between the bare band structures obtained in theoretical
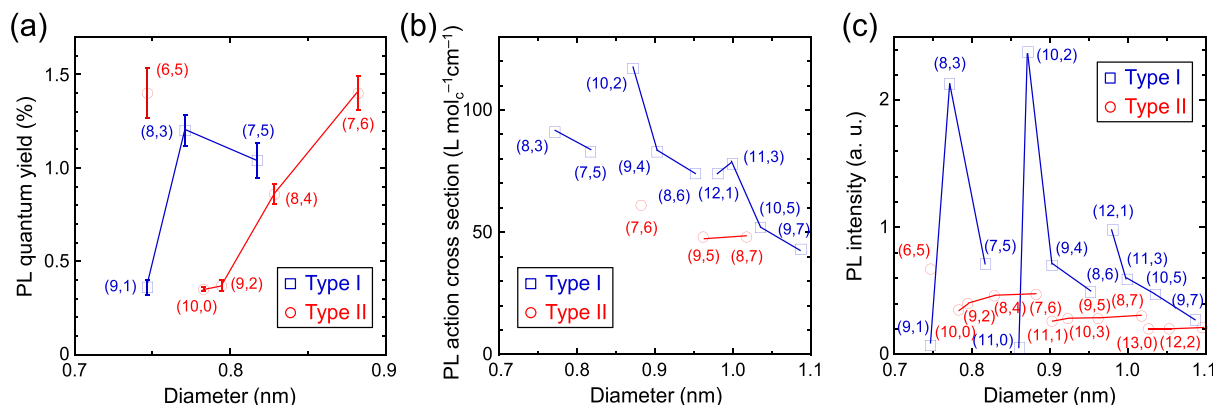

Figure 5. (a) Plots of the PL quantum yields of eight (n,m) SWCNTs as a function of SWCNT diameter. Error bars show the uncertainties shown in Table 1. (b) Plots of the PL action cross section from ref 12 as a function of the SWCNT diameter. (c) Plots of the PL intensity from ref 11 as a function of the SWCNT diameter. Type I and Type II species are denoted as blue squares and red circles, respectively. The symbols corresponding to the chiralities with the same family number ($2n + m$) are connected to guide the eye.

calculations[42] and the excitonic band structures obtained in experiments[17] for (9,1) and (8,3) species if the PL quantum yields of the SWCNTs are also dominated by their relaxation rates. We also have to consider other possible reasons because the PL intensities and quantum yields of SWCNTs are highly influenced by their lengths, surrounding environments, and qualities. In the present experiment, the PL quantum yield was quantified for the SWCNTs with a specific length distribution in a surfactant solution; in contrast, in the theoretical calculation, the relative PL intensity was quantified for SWCNTs with a unit length in a vacuum. It should be mentioned that the chiral SC surfactant was used to disperse the SWCNTs in this work. In principle, chiral molecule or DNA may result in a difference in PL quantum yield between two enantiomers of the specific (n,m) SWCNTs due to handedness-dependent interactions with the chiral molecule.[43,44] However, difference in the PL quantum yield between two enantiomers dispersed in SC solution was 4.2% that is smaller than the value of 9.8% for achiral sodium dodecyl benzenesulfonate (Supporting Information, Figure S16). In addition, the SWCNTs used in the theoretical calculation had perfect covalent sp^2 bonds between individual carbon atoms; in contrast, the SWCNTs measured in the present experiment actually have several defect sites induced by the SWCNT dispersion process. Although we performed the same dispersion process, the ease of introducing defects should be different for individual chiralities, which is likely to depend on the structure of the SWCNTs, such as the diameter.[31] It is important to note that the PL intensity and quantum yield of the E_{11} transition significantly decrease after the introduction of defects due to the change of the phonon lifetime.[45] Previous studies have demonstrated that the intensity and position of the defect-derived PL peak changed depending on the structure of the SWCNTs.[28,29,31] This change suggests the possibility that the defect-induced reductions in the PL intensity and quantum yield depend on the structure of the SWCNTs, but the detailed dependence is not investigated in this work. As mentioned above, therefore, the factors of SWCNT length, surrounding environment, and quality can account for the quantitative discrepancy between the experiment and theoretical calculation. However, a clear family pattern fully demonstrates that the diameter, chiral angle, and type play an important role in the PL quantum yield of semiconducting SWCNTs, which is very useful for a deeper understanding of the photophysical properties of SWCNTs.

In conclusion, we found that photon reabsorption highly modified the PL spectra of SWCNTs. By taking the photon reabsorption effect into consideration, we demonstrated that the PL quantum yields strongly depend on the SWCNT structure, including the family, diameter, and chiral angle, indicating that the apparent PL intensities do not represent the correct (n,m) distribution. For quantitative evaluation of the (n,m) distribution in SWCNT samples, not only the structure-dependent quantum yields obtained in this study but also the intensity correction for the reabsorption effect are found to be very important.

ASSOCIATED CONTENT

Ⓢ Supporting Information

The Supporting Information is available free of charge at https://pubs.acs.org/doi/10.1021/acs.nanolett.9b04095.

Details of optical measurements, effects of enantiomers, PL spectral characteristics of eight (n,m) species, influence of solvent, estimated PL quantum yields per unit of absorbed photons, and fitting equation for integrals of observed PL intensity (PDF)

AUTHOR INFORMATION

Corresponding Author

*Email: h-kataura@aist.go.jp.

ORCID Ⓞ

Takeshi Tanaka: 0000-0001-7547-7928
Shilong Li: 0000-0002-6355-7143
Yohei Yomogida: 0000-0002-8569-6179
Atsushi Hirano: 0000-0002-4138-0308
Huaping Liu: 0000-0001-7017-4127
Hiromichi Kataura: 0000-0002-4777-0622

Notes

The authors declare no competing financial interest.

REFERENCES

(1) Wilder, J. W. G.; Venema, L. C.; Rinzler, A. G.; Smalley, R. E.; Dekker, C. Electronic structure of atomically resolved carbon nanotubes. *Nature* **1998**, *391*, 59−62.

(2) Bachilo, S. M.; Strano, M. S.; Kittrell, C.; Hauge, R. H.; Smalley, R. E.; Weisman, R. B. Structure-assigned optical spectra of single-walled carbon nanotubes. *Science* **2002**, *298*, 2361−2366.

(3) Okazaki, T.; Saito, T.; Matsuura, K.; Ohshima, S.; Yumura, M.; Oyama, Y.; Saito, R.; Iijima, S. Photoluminescence and population analysis of single-walled carbon nanotubes produced by CVD and pulsed-laser vaporization methods. *Chem. Phys. Lett.* **2006**, *420*, 286−290.

(4) Jorio, A.; Fantini, C.; Pimenta, M.; et al. Carbon nanotube population analysis from Raman and photoluminescence intensities. *Appl. Phys. Lett.* **2006**, *88*, No. 023109.

(5) Li, X.; Tu, X.; Zaric, S.; Welsher, K.; Seo, W. S.; Zhao, W.; Dai, H. Selective synthesis combined with chemical separation of single-walled carbon nanotubes for chirality selection. *J. Am. Chem. Soc.* **2007**, *129*, 15770−15771.

(6) Ju, S. Y.; Doll, J.; Sharma, I.; Papadimitrakopoulos, F. Selection of carbon nanotubes with specific chiralities using helical assemblies of flavin mononucleotide. *Nat. Nanotechnol.* **2008**, *3*, 356−362.

(7) Chiang, W. H.; Sankaran, R. M. Linking catalyst composition to chirality distributions of as-grown single-walled carbon nanotubes by tuning Ni_xFe_{1-x} nanoparticles. *Nat. Mater.* **2009**, *8*, 882−886.

(8) He, M.; Chernov, A. I.; Fedotov, P. V.; Obraztsova, E. D.; Sainio, J.; Rikkinen, E.; Jiang, H.; Zhu, Z.; Tian, Y.; Kauppinen, E. I.; Niemelä, M.; Krause, A. O. I. Predominant (6,5) single-walled carbon nanotube growth on a copper-promoted iron catalyst. *J. Am. Chem. Soc.* **2010**, *132*, 13994−13996.

(9) Wang, H.; Wang, B.; Quek, X. Y.; Wei, L.; Zhao, J.; Li, L. J.; Chan-Park, M. B.; Yang, Y.; Chen, Y. Selective synthesis of (9,8) single walled carbon nanotubes on cobalt incorporated TUD-1 catalysts. *J. Am. Chem. Soc.* **2010**, *132*, 16747−16749.

(10) Wang, H.; Wei, L.; Ren, F.; Wang, Q.; Pfefferle, L. D.; Haller, G. L.; Chen, Y. Chiral-selective $CoSO_4/SiO_2$ catalyst for (9,8) single-walled carbon nanotube growth. *ACS Nano* **2013**, *7*, 614−626.

(11) Oyama, Y.; Saito, R.; Sato, K.; Jiang, J.; Samsonidze, G. G.; Grüneis, A.; Miyauchi, Y.; Maruyama, S.; Jorio, A.; Dresselhaus, G.; Dresselhaus, M. S. Photoluminescence intensity of single-wall carbon nanotubes. *Carbon* **2006**, *44*, 873−879.

(12) Tsyboulski, D. A.; Rocha, J. D. R.; Bachilo, S. M.; Cognet, L.; Weisman, R. B. Structure-dependent fluorescence efficiencies of individual single-walled carbon nanotubes. *Nano Lett.* **2007**, *7*, 3080−3085.

(13) Mouri, S.; Miyauchi, Y.; Matsuda, K. Dispersion-process effects on the photoluminescence quantum yields of single-walled carbon nanotubes dispersed using aromatic polymers. *J. Phys. Chem. C* **2012**, *116*, 10282−10286.

(14) Ahn, T. S.; Al-Kaysi, R. O.; Müller, A. M.; Wentz, K. M.; Bardeen, C. J. Self-absorption correction for solid-state photoluminescence quantum yields obtained from integrating sphere measurements. *Rev. Sci. Instrum.* **2007**, *78*, No. 086105.

(15) Zhang, N.; Dai, D.; Zhang, W.; Fan, J. Photoluminescence and light reabsorption in SiC quantum dots embedded in binary-polyelectrolyte solid matrix. *J. Appl. Phys.* **2012**, *112*, No. 094315.

(16) Zhang, W.; Dai, D.; Chen, X.; Guo, X.; Fan, J. Red shift in the photoluminescence of colloidal carbon quantum dots induced by photon reabsorption. *Appl. Phys. Lett.* **2014**, *104*, No. 091902.

(17) Wei, X.; Tanaka, T.; Yomogida, Y.; Sato, N.; Saito, R.; Kataura, H. Experimental determination of excitonic band structures of single-walled carbon nanotubes using circular dichroism spectra. *Nat. Commun.* **2016**, *7*, 12899.

(18) Yomogida, Y.; Tanaka, T.; Zhang, M.; Yudasaka, M.; Wei, X.; Kataura, H. Industrial-scale separation of high-purity single-chirality single-wall carbon nanotubes for biological imaging. *Nat. Commun.* **2016**, *7*, 12056.

(19) Wei, X.; Tanaka, T.; Hirakawa, T.; Wang, G.; Kataura, H. High-efficiency separation of (6,5) carbon nanotubes by stepwise elution gel chromatography. *Phys. Status Solidi B* **2017**, *254*, 1700279.

(20) Wei, X.; Tanaka, T.; Hirakawa, T.; Yomogida, Y.; Kataura, H. Determination of enantiomeric purity of single-wall carbon nanotubes using flavin mononucleotide. *J. Am. Chem. Soc.* **2017**, *139*, 16068−16071.

(21) Liu, H.; Nishide, D.; Tanaka, T.; Kataura, H. Large-scale single-chirality separation of single-wall carbon nanotubes by simple gel chromatography. *Nat. Commun.* **2011**, *2*, 309.

(22) Liu, H.; Tanaka, T.; Urabe, Y.; Kataura, H. High-efficiency single-chirality separation of carbon nanotubes using temperature-controlled gel chromatography. *Nano Lett.* **2013**, *13*, 1996−2003.

(23) Flavel, B. S.; Kappes, M. M.; Krupke, R.; Hennrich, F. Separation of single-walled carbon nanotubes by 1-dodecanol-mediated size-exclusion chromatography. *ACS Nano* **2013**, *7*, 3557−3564.

(24) Tvrdy, K.; Jain, R. M.; Han, R.; Hilmer, A. J.; McNicholas, T. P.; Strano, M. S. A kinetic model for the deterministic prediction of gel-based single-chirality single-walled carbon nanotube separation. *ACS Nano* **2013**, *7*, 1779−1789.

(25) Kataura, H.; Kumazawa, Y.; Maniwa, Y.; Umezu, I.; Suzuki, S.; Ohtsuka, Y.; Achiba, Y. Optical properties of single-wall carbon nanotubes. *Synth. Met.* **1999**, *103*, 2555−2558.

(26) Weisman, R. B.; Bachilo, S. M. Dependence of optical transition energies on structure for single-walled carbon nanotubes in aqueous suspension: an empirical Kataura plot. *Nano Lett.* **2003**, *3*, 1235−1238.

(27) Everall, N. Quantitative study of self-absorption in near-infrared Fourier transform Raman spectroscopy. *J. Raman Spectrosc.* **1994**, *25*, 813−819.

(28) Ghosh, S.; Bachilo, S. M.; Simonette, R. A.; Beckingham, K. M.; Weisman, R. B. Oxygen doping modifies near-infrared band gaps in fluorescent single-walled carbon nanotubes. *Science* **2010**, *330*, 1656−1659.

(29) Piao, Y.; Meany, B.; Powell, L. R.; Valley, N.; Kwon, H.; Schatz, G. C.; Wang, Y. Brightening of carbon nanotube photoluminescence through the incorporation of sp^3 defects. *Nat. Chem.* **2013**, *5*, 840−845.

(30) Miyauchi, Y.; Iwamura, M.; Mouri, S.; Kawazoe, T.; Ohtsu, M.; Matsuda, K. Brightening of excitons in carbon nanotubes on dimensionality modification. *Nat. Photonics* **2013**, *7*, 715−719.

(31) Wei, X.; Tanaka, T.; Akizuki, N.; Miyauchi, Y.; Matsuda, K.; Ohfuchi, M.; Kataura, H. Single-chirality separation and optical properties of (5,4) single-wall carbon nanotubes. *J. Phys. Chem. C* **2016**, *120*, 10705−10710.

(32) Ohfuchi, M.; Miyamoto, Y. Optical properties of oxidized single-wall carbon nanotubes. *Carbon* **2017**, *114*, 418−423.

(33) Ohno, Y.; Iwasaki, S.; Murakami, Y.; Kishimoto, S.; Maruyama, S.; Mizutani, T. Chirality-dependent environmental effects in photoluminescence of single-walled carbon nanotubes. *Phys. Rev. B: Condens. Matter Mater. Phys.* **2006**, *73*, 235427.

(34) Crochet, J.; Clemens, M.; Hertel, T. Quantum yield heterogeneities of aqueous single-wall carbon nanotube suspensions. *J. Am. Chem. Soc.* **2007**, *129*, 8058−8059.

(35) Hirana, Y.; Tanaka, Y.; Niidome, Y.; Nakashima, N. Strong micro-dielectric environment effect on the band gaps of (n,m) single-walled carbon nanotubes. *J. Am. Chem. Soc.* **2010**, *132*, 13072−13077.

(36) Streit, J. K.; Bachilo, S. M.; Ghosh, S.; Lin, C. W.; Weisman, R. B. Directly measured optical absorption cross sections for structure-selected single-walled carbon nanotubes. *Nano Lett.* **2014**, *14*, 1530−1536.

(37) Sanchez, S. R.; Bachilo, S. M.; Kadria-Vili, Y.; Lin, C. W.; Weisman, R. B. (n,m)-specific absorption cross sections of single-walled carbon nanotubes measured by variance spectroscopy. *Nano Lett.* **2016**, *16*, 6903−6909.

(38) Choi, S.; Deslippe, J.; Capaz, R. B.; Louie, S. G. An explicit formula for optical oscillator strength of excitons in semiconducting single-walled carbon nanotubes: family behavior. *Nano Lett.* **2013**, *13*, 54−58.

(39) Miyauchi, Y.; Hirori, H.; Matsuda, K.; Kanemitsu, Y. Radiative lifetimes and coherence lengths of one-dimensional excitons in single-walled carbon nanotubes. *Phys. Rev. B: Condens. Matter Mater. Phys.* **2009**, *80*, No. 081410.

(40) Hertel, T.; Himmelein, S.; Ackermann, T.; Stich, D.; Crochet, J. Diffusion limited photoluminescence quantum yields in 1-D semiconductors: single-wall carbon nanotubes. *ACS Nano* **2010**, *4*, 7161−7168.

(41) Graf, A.; Zakharko, Y.; Schießl, S. P.; Backes, C.; Pfohl, M.; Flavel, B. S.; Zaumseil, J. Large scale, selective dispersion of long single-walled carbon nanotubes with high photoluminescence quantum yield by shear force mixing. *Carbon* **2016**, *105*, 593−599.

(42) Samsonidze, G. G.; Saito, R.; Kobayashi, N.; Grüneis, A.; Jiang, J.; Jorio, A.; Chou, S. G.; Dresselhaus, G.; Dresselhaus, M. S. Family behavior of the optical transition energies in single-wall carbon nanotubes of smaller diameters. *Appl. Phys. Lett.* **2004**, *85*, 5703−5705.

(43) Ao, G.; Streit, J. K.; Fagan, J. A.; Zheng, M. Differentiating left- and right-handed carbon nanotubes by DNA. *J. Am. Chem. Soc.* **2016**, *138*, 16677−16685.

(44) Zheng, Y.; Bachilo, S. M.; Weisman, R. B. Enantiomers of single-wall carbon nanotubes show distinct coating displacement kinetics. *J. Phys. Chem. Lett.* **2018**, *9*, 3793−3797.

(45) Miyauchi, Y.; Matsuda, K.; Yamamoto, Y.; Nakashima, N.; Kanemitsu, Y. Length-dependent photoluminescence lifetimes in single-walled carbon nanotubes. *J. Phys. Chem. C* **2010**, *114*, 12905−12908.